

# Simulating Prostate Surgical Procedures with a Discrete Soft Tissue Model

Maud Marchal<sup>1</sup> and Emmanuel Promayon<sup>1</sup> and Jocelyne Troccaz<sup>1</sup>

<sup>1</sup>Laboratoire TIMC, Equipe GMCAO  
Institut d'Ingénierie de l'Information de Santé  
38706 LA TRONCHE Cedex

---

## Abstract

*Simulating surgical procedures is still a complex challenge. Either modeling methods or simulators have to take into account specific geometries and properties of the patient organs. In this paper, a new soft tissue modeling method dedicated to prostate surgical interventions is presented. The chosen medical application requires the modeling of a complex anatomical environment including intricate interactions between organs and surgical instruments. We present a discrete model that has been specifically developed to fulfill these requirements. The influence of two particular instruments is studied: needles and ultrasound probe, according to two surgical interventions: biopsy and brachytherapy.*

Categories and Subject Descriptors (according to ACM CCS): I.3.5[COMPUTER GRAPHICS]: Physically based modeling I.6.8 [SIMULATION AND MODELING]: Animation

---

**Keywords:** Physically-based model, medical simulation, discrete model, prostate surgery, needle insertion modeling

## 1. Introduction

Prostate cancer is nowadays the most diagnosed cancer among men in developed countries. Over the last ten years, the number of medical procedures to treat this cancer has considerably increased. Different categories of medical interventions can be distinguished, according to their objectives. In this paper, we are interested in two particular interventions: biopsy and brachytherapy. Biopsy is the most common way to diagnose prostate cancer. It consists in introducing a needle through the rectum wall to take tissue samples. To treat prostate cancer, different options are possible in function of the cancer stage. The main treatments are radiotherapy and surgery. New promising procedures have been recently developed. Among them, brachytherapy takes an increasing place as it is less invasive and thus yields to faster recovering than previous treatments. The brachytherapy procedure consists in introducing radioactive seeds in

the prostate through needles. The Figures 1 and 2 detail the spatial configurations of the two studied procedures.

For both brachytherapy and biopsy, the surgical operations are conducted with the help of ultrasound imaging acquired by an endorectal probe. Poor quality of images as well as movements and deformations of the tissues (prostate and its surrounding organs) are the main limiting factors of the efficiency and result quality of these interventions. A better comprehension of prostate deformations in the anatomical environment could improve the planning of medical interventions and the training of physicians. This can be achieved through the development of medical simulators capable of modeling both deformations of organs and interactions with the instruments. In this paper, we propose a discrete model to simulate the interactions with the prostate in order to train the surgeon to apprehend prostate deformations and movements during medical procedures.

As of today a few computer-based training systems focused on the modeling of complex anatomical environment have been developed. These systems include the complete modeling of a given organ but do not deal with the complex

interactions between a surgical tool and an organ as well as the interactions between organs themselves. In this paper, we propose a model belonging to the category of discrete models in order to simulate both external and internal interactions. It owns a specific formulation of the elasticity, using a volumetric local shape memory. The description of the components of each set of organs allows to easily define interactions both with external elements like surgical tools and internal elements like the surrounding organs of the prostate. In this paper, we focus on two particular surgical tools mainly used in prostate medical procedures: needles and ultrasound probe.

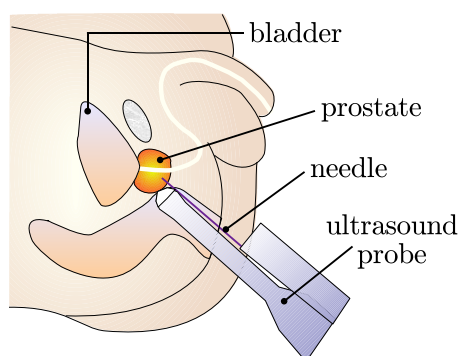


**Figure 1:** Description of a prostate biopsy.

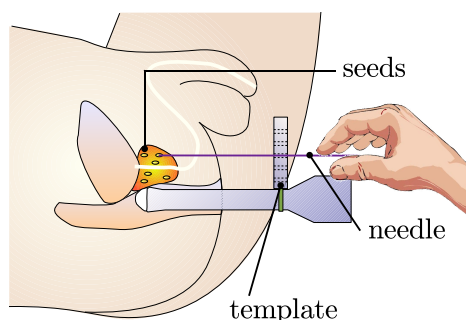


**Figure 2:** Description of a prostate brachytherapy.

This paper is organized as follows: previous work is discussed in section 2, then our modeling method is outlined in section 3. In section 4, the modeling of interactions is detailed. Medical simulations are presented in section 5.

## 2. Simulation of Soft Tissue Interactions in a Surgical Environment

Simulations of anatomical models have been particularly published these last years. The physician need for practicing his gestures as well as the possibility to realize a pre-operative surgical planning are the main reasons for this development. Concerning the anatomy of the models, it is often

reduced to a particular organ without taking into account the surrounding organs.

Few models concern the modeling of the prostate and its environment, which mainly includes the bladder and the rectum. For example, [MDT02] have proposed a combination of a statistical and a biomechanical model to simulate the deformations of the prostate due to an ultrasound probe. Their model is based on Finite Element Method (FEM) and is composed of a prostate and its near environment. The influence of surrounding organs geometries is not coupled with the study of ultrasound probe. [PA04] have developed a 3D model based on mass-springs to simulate the prostate resection. Only the prostate and its interactions with surgical tools are represented.

The modeling of surgical tools around the prostate has been studied for different objects, mainly the ultrasound probe [MDT02] and cutting tools [PA04]. Concerning the needle insertion modeling, models have been firstly developed in 2D [APT\*03, DS05] and recently extended in 3D [GSD\*05]. Tissue deformations and surgical planning have also been studied thanks to FEM using geometric non-linearity [DS05]. The modeling of the needle itself has been realized with linear beam elements [GS04] or by identifying a non-holonomic model for a highly flexible needle in order to simulate the effect of its bevel tip [IKC\*06]. The first results of [ICCO04] have been used by [AGCO05] for path planning of a needle in 2D tissue. No organ modeling is currently combined with these needle simulations.

The objectives of our model are to combine both external influences (surgical tools like needles or ultrasound probe) and internal influences (surrounding organs) to help the surgeon to understand prostate movements and deformations during biopsy and brachytherapy. We chose to build a new discrete model in order to easily define several interactions between objects with different physical properties.

## 3. Description of the Discrete Soft Tissue Model

The model belongs to the category of discrete models. Firstly, the description of the modeling framework is detailed and its different properties are explained. The elasticity property, defined thanks to a local shape memory, is then described. Finally, a paragraph is devoted to the volume preservation in the model.

### 3.1. Model Description

Distinct components, such as skeleton, soft tissues and muscles, and their connections and interactions can be handled by our modeling framework. Each component has its own geometry and physical properties, including mass, elasticity and activation function.

Each component is defined by a set of nodes or particles. Each particle has a position, a neighborhood and different

properties depending on what kind of component it belongs to. No specific mesh (e.g. triangles, tetrahedra, hexahedra) is needed. The particles are either at the surface or inside a component. A mass is assigned to each particle in order to generate forces and dynamics.

Each component can be modeled by a surface description (particles are only on the component boundary) or with a volumetric description (particles are also present inside the component), depending on their physical properties and on the level of details to achieve.

Living structures are governed by three main kinds of components: rigid components to model skeleton, deformable components to model soft tissues and active deformable components to model muscles. The latter inherits deformable components properties.

In our model, components with different properties can be easily assembled together. This allows us to define complex interactions for a given anatomical environment. For example, interactions between two elastic components or two rigid components or between an elastic and a rigid component can be modeled. For the latter, border particles of solid and elastic components are doubled but constrained to be at the same position, whatever forces are applied on them. The forces generated by an elastic (active) component can thus be transmitted to a solid component, for example to model a tendinous link between a bone and a muscle. For solid interactions, the link between two components can be modeled thanks to an elastic component, for example to model two bones linked by a ligament. Figure 3 illustrates the interaction between three soft organs.

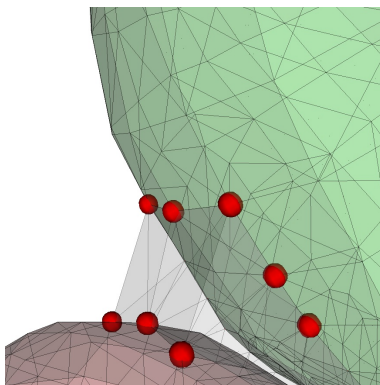


**Figure 3:** Example of an interaction between elastic components with three kind of soft tissues : prostate (bottom), bladder (top) and intermediate fat tissue (transparent). Border particles belong to only one of the component but have neighbors in the other elastic component.

Besides the geometrical description, forces acting on each component and generating displacements and deformations have to be considered. Three kinds of forces can be used in

the model: force fields (e.g. gravitation force), locally applied forces (e.g. forces generated by the user interaction) and internal forces (e.g. local shape memory forces to model deformable properties and active fiber forces to model muscular activity).

In addition to forces, constraints have to be implemented to model complex behaviors and to maintain some conditions such as non-penetrating volume. Our model can deal with two kinds of constraints:

- local constraints that are applied to a single particle, for example to keep a particle in a specific region of space,
- global constraints that are applied to a set of particles, for example to enforce incompressibility.

The algorithm considers constraints as non-quantified forces: their satisfaction is guaranteed by using a direct projection algorithm based on the gradient vector of the constraint function. Volume preservation can be satisfied using this method and the algorithm is detailed in a next paragraph.

To solve the system dynamics, at each time  $t$ , the forces on each particle are summed and the equations of motion are integrated taking into account the local and global constraints. The discrete integration scheme used for the equation of motion is an explicit scheme. The different steps of one iteration of the algorithm are detailed in the algorithm 1.

---

**Algorithm 1:** General algorithm of the model

---

```

foreach component of the global model do
  | foreach particle of the component do
  | | applyBoundaryConditions();
  | end
end
foreach component of the global model do
  | foreach particle of the component do
  | | computeAllForces();
  | | redistributeInternalForces();
  | end
end
foreach component of the global model do
  | foreach particle of the component do
  | | sumForces();
  | | computeNewPosition();
  | | applyConstraints();
  | | adjustVelocity();
  | end
end

```

---

### 3.2. Soft Tissue Modeling

This paragraph is dedicated to the description of the soft tissue modeling method in our model. In the litterature, elasticity of a soft tissue model is introduced and defined by different ways depending on the chosen modeling method. The

elasticity property of an object is its ability to come back to its initial shape once deformed. In a mass-spring system for example, the combination of springs exerting forces on masses allows the object to recover its initial shape. In our model, a shape memory force is defined for each particle to achieve the elasticity property.

### 3.2.1. Shape Memory Principle

In the model, a shape memory force is used on each elastic particle. Each particle has a shape *attractor*. The position  $\mathbf{P}^*$  of this attractor is defined thanks to a shape function  $f$  of the particle neighbors positions. At rest configuration, when there is no deformation,  $f$  is defined so that the shape attractor is at the same position as the particle which position is noted  $\mathbf{P}$ . Hence when there is no deformation,  $\mathbf{P}^*$  and  $\mathbf{P}$  have the same coordinates. If one or all the neighbors move,  $\mathbf{P}^*$  changes according to  $f$ . A shape memory force  $\mathbf{F}^*$  is generated on the particle in order to move it towards its shape attractor. If a particle and its attractor are at the same position, then the shape memory force  $\mathbf{F}^*$  is null. A 3D example is shown in Figure 4.

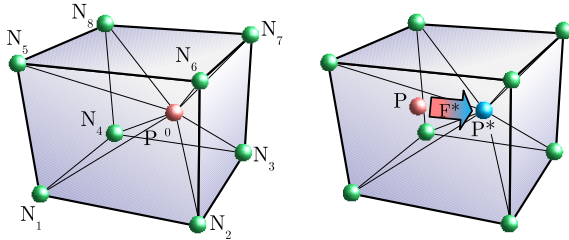


**Figure 4:** At rest position, the shape attractor is defined so that  $\mathbf{P}^* = \mathbf{P}^0$  (left). During the simulation, the particle has moved to position  $\mathbf{P}$  (right). A shape memory force  $\mathbf{F}^*$  is applied to the particle "attracting" it towards its shape attractor position  $\mathbf{P}^*$ . If the particle neighbors have not moved, the attractor is still in  $\mathbf{P}^* = \mathbf{P}^0$ .

The shape memory force is defined as a vector between the current particle position and the position of its shape attractor, multiplied by an elasticity stiffness weight  $k_e$ :  $\mathbf{F}^* = k_e(\mathbf{P}^* - \mathbf{P})$ , which corresponds to a direct linear actuator between  $\mathbf{P}^*$  and  $\mathbf{P}$ . Each particle  $i$  can hold a local stiffness  $k_e^i$ . According to Newton's second law, the opposite force of this shape memory force is redistributed to the neighbors depending on  $f$ .

### 3.2.2. Attractor Function

Unlike [MHTG05] where the particle displacements are found with a minimization process, the position of a particle attractor is expressed as a function  $f$  of the neighbor particles. The function  $f$  can be seen as an extension of the barycentric coordinates. Barycentric coordinates are unique for triangles in 2D or tetrahedra in 3D but there are many different generalizations for polygons in 2D and polyhedra in

3D. They are more and more often used in computer graphics to express a point as a convex combination of the vertices of a tetrahedra. The generalization of the expressions of these coordinates to convex polygons recently has become a quite hot research topic. Floater et al. [FHK06] give a summary of the existing methods. But the extension of these equations to non-convex polygons is currently available only for star-shaped polygons and do not satisfy enough conditions, e.g. non negative weights. The method presented in this paper can be used to find the coordinates of a 3D point as a function of neighborhood points either for convex or non-convex polyhedra. The next paragraph details the computation of an attractor position.

### 3.2.3. Discrete Deformation Coordinates

The idea is to compute the coordinates of a point in 3D relatively to other 3D points. We have to consider all the possible directions defined by the neighbor positions. Deformation for a particle is computed as the barycenter of all possible discrete deformations.

Let  $\mathbf{P}$  be the position of the particle of interest. Let  $\mathbf{N}_i$ ,  $i \in [1 \dots n]$  be the positions of the  $n$  neighbors of this particle. Each triplet  $\langle \mathbf{N}_i, \mathbf{N}_j, \mathbf{N}_k \rangle$  with  $i \neq j \neq k$  and  $i, j, k \in [1 \dots n]$  forms a triangle  $\mathbf{t}$  of normal denoted  $\mathbf{n}_t$ .

We can define  $\mathbf{P}$  relatively to triplet  $\langle \mathbf{N}_i, \mathbf{N}_j, \mathbf{N}_k \rangle$ , noted  $\mathbf{P}_t$  by:

$$\mathbf{P}_t = \mathbf{Q}_t + \beta_t \frac{\mathbf{n}_t}{\|\mathbf{n}_t\|} \quad (1)$$

where  $\mathbf{Q}_t$  is the projection of  $\mathbf{P}$  on  $\langle \mathbf{N}_i, \mathbf{N}_j, \mathbf{N}_k \rangle$  along  $\mathbf{n}_t$ , with  $\beta_t$  the distance between  $\mathbf{Q}_t$  and  $\mathbf{P}$  (see Figure 5).  $\mathbf{Q}_t$  can be defined using the barycentric coordinates as:

$$\mathbf{Q}_t = \alpha_i^i \cdot \mathbf{N}_i + \alpha_j^j \cdot \mathbf{N}_j + \alpha_k^k \cdot \mathbf{N}_k \quad (2)$$

At each time step,  $\mathbf{P}_t$  can be considered as a measure of the discrete deformation of triplet  $t$ .

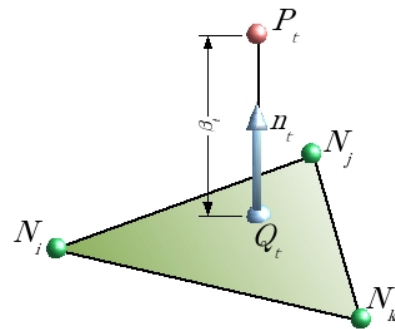


**Figure 5:**  $\mathbf{P}_t$  can be defined relatively to triplet  $\langle \mathbf{N}_i, \mathbf{N}_j, \mathbf{N}_k \rangle$  by its projection  $\mathbf{Q}_t$  along the normal  $\mathbf{n}_t$ .

Thus, we can define the attractor  $\mathbf{P}^*$  as the isobarycenter of all the  $\mathbf{P}_t$  resulting from the  $m$  valid triplets by:

$$\mathbf{P}^* = \frac{1}{m} \sum_{t=1}^{t=m} \left( \mathbf{Q}_t + \beta_t \frac{\mathbf{n}_t}{\|\mathbf{n}_t\|} \right) \quad (3)$$

where  $t$  is the index of a valid triplet  $\langle \mathbf{N}_i, \mathbf{N}_j, \mathbf{N}_k \rangle$ .  $\mathbf{P}^*$  is called the discrete deformation coordinate.

Note that not all  $C_n^3$  triplets are valid, triplets resulting in a line are rejected (thus  $m < C_n^3$ ). Also note that as  $\mathbf{Q}_t$  is defined using the classical barycentric coordinates, thus  $\alpha_t^i + \alpha_t^j + \alpha_t^k = 1$ . At each iteration, the new normal of each triplet with  $\beta_t \neq 0$  has to be computed to obtain the new attractor position. The part of the force redistributed to each neighboring particles is proportional to the linear coefficient of the attractor formulation.

The discrete deformation coordinates gives a good evaluation of a discrete local deformation in all neighbor directions only using the neighbor positions.

### 3.3. Volume Preservation

Volume preservation is an essential part of soft tissue modeling. The control of the volume is necessary in order to simulate both the incompressibility of given organs and the volume variation of other organs like bladder for example. The computation of the volume constraint is described in this paragraph in the case of a 3D object.

The incompressibility constraint is applied on the particles belonging to the surface of the 3D object. These particles can be represented by a polyhedron of  $n$  vertices. This polyhedron is pre-computed and is also used for visualization. Let  $\mathbf{P}_1, \dots, \mathbf{P}_n$  be the positions of these vertices and  $F_1, \dots, F_m$  the  $m$  faces describing the surface. Let  $\mathbf{X}$  be the vector of size  $3n$  holding the positions of all the vertices:  $\mathbf{X} = (\mathbf{P}_1, \dots, \mathbf{P}_n)$ .

Let  $V(\mathbf{X})$  be a function giving the volume defined by the polyhedron. Let  $V_0$  be the value of the initial volume. Supposing that the user has manipulated the object, resulting in a deformed polyhedron of vertices position  $\mathbf{X}'$ , our method provides a quick way to find a polyhedron of state vector  $\mathbf{X}^1$ , "similar" to the polyhedron of state vector  $\mathbf{X}'$ . Our constraint resolution implies to find the displacements to apply to each vertex. The following system has to be solved:

$$\begin{cases} \mathbf{X}^1 &= \mathbf{X}' + \lambda \nabla V(\mathbf{X}') \\ V(\mathbf{X}^1) &= V_0 \end{cases} \quad (4)$$

where  $\nabla V(\mathbf{X})$  is the gradient of the volume function  $V(\mathbf{X})$  (i.e. the constraint field derivative) and  $\lambda$  is a scalar. Solving equation 4 allows us to find a solution for the volume-preservation problem directly, in one pass. Note that in the more general case of a non polyhedral representation, if the

representation allows us to compute the volume and its gradient, then this method can also be used and consists in solving a system of  $3n+1$  equations of  $3n+1$  unknowns:  $\mathbf{X}^1$  and  $\lambda$ . Compared to lagrangian methods (lagrangian multiplier and/or minimization algorithm), our method exactly solves the constraint.

### 3.4. Validation of the Model

Discrete models are known to have effective computational properties but to be less accurate than FEM for example. Concerning our model, its performances have been validated against other soft tissue modeling methods by using comparisons with real data like Truth Cube experiment [KCO\*03]. The results of the comparisons are available in [MPT05] and show a similar behavior as FEM for different levels of compression of the Truth Cube.

## 4. Description of a Surgical Environment

### 4.1. Interactions between Organs and Surgical Instruments

The interactions between organs and surgical instruments are included in our model. In the context of prostate surgical interventions, the main instrument is the endorectal ultrasound probe. Displacements constraints are applied on the organs of the patient. These constraints can be modified during the simulation, for example to simulate a translation or a rotation applied by the surgeon on the ultrasound probe.

In this paper, we focus on two particular interventions around the prostate but other surgical tools can also be defined in the same manner.

### 4.2. Needle Insertion Modeling

In this paper, only the simulation of rigid needles is explained. Two examples of needle insertion modeling are represented in figures 6 and 8.

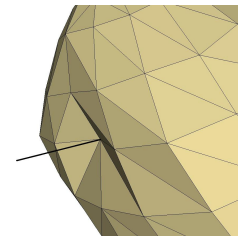


Figure 6: Details of needle insertion in a prostate.

#### 4.2.1. Model

Rather than modeling the needle as a distinct object and dealing with collision detections, only the forces between the needle and the soft tissue are simulated directly, as explained

in this paragraph. This hypothesis has previously been used with success by [AGO05, DS03, ICCO04, GSD\*05]. The needle is only defined by a set of aligned nodes.

The forces applied on a tissue during needle insertion can be divided in three different forces [SO02]: (a) cutting force: the needle tip exerts a force in order to move through the tissue, (b) puncture force: the force needed to puncture a tissue, generally much higher than the cutting force due to the surface tension or the presence of a capsule, (c) friction force: it is applied along the needle shaft.

These forces are computed and applied on the tissue but depends on the type of the needle and its insertion velocity as well as the tissue properties. The reaction forces from the tissue have also to be computed to simulate the movement of the needle.

Contrary to FEM models [AGO05, DS03], forces are not applied as boundary conditions for the elements of the tissue mesh. As we are using a discrete model, forces can be applied directly on the particles. Our discrete method do not need any remesh stage in order to ensure that element boundaries are present when forces are applied. The needle can thus be inserted in any location of the tissue without extra cost. Forces on tissue particles are applied depending on their location relatively to the needle, as explained in the next paragraph.

**Zones of interest** Two types of zones of interest are defined around the needle: the cutting zone and the friction zones. A zone of interest defines a spatial volume where all tissue particles are directly subject to the influence of the considered force. Its dimensions are defined as parameters of the needle model. For example, it is possible to define the dimensions of the zones of interest so that the friction along the needle decreases in function of the distance to the needle shaft. A description of the zones of interest is given in Figure 7. The cutting zone is defined in front of the needle tip node only. When the needle is not yet inserted inside the tissue, the cutting zone is also the puncture zone. The friction zones are defined all around each needle node. There is one friction zone per needle node.

All tissue particles entering in these zones will be concerned by the corresponding forces coming from the needle. During the simulation, after the first collision between the tip node and the tissue has been detected, the initial zones of interest are built. Then, the zones of interest are moved depending on the needle displacement. The list of tissue particles inside the different zones is efficiently updated by only checking the neighbors of the particles already in the zones at each time step.

**Tissue parameters** Friction and cutting parameters are different for each soft tissue. They can not be easily found and we used DiMaio et al. [DS03] data to tune our parameters. Similarly to the elasticity parameter  $k_e$ , each particle has friction and cutting force parameters defined as weights

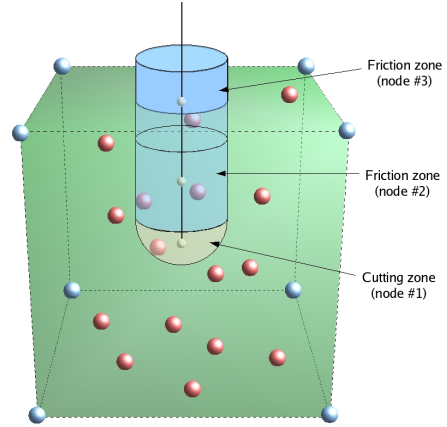


**Figure 7:** Volumes of interest: needle nodes (white) have a friction zone (blue) with tissue particles inside. The needle tip has a cutting zone (grey).

and named respectively  $k_f$  and  $k_c$ : the higher the values of  $k_f$  and  $k_c$ , the higher the resistance of the tissue to the friction and cutting forces. The accurate values of these parameters have been determined by [SO02, DS03]. The parameters used in our simulation have been tuned to provide realistic simulations. Note that these values are dependant of the needle velocity. Each tissue particle can have different friction and cutting force weights in order to model a local change inside a tissue (for example to model a tumour inside an organ with different parameters).

In the next paragraphs, details of implementation of the three different forces and their parameters are provided.

**Cutting force** The cutting force is applied by the needle on all the  $n$  tissue particles located in the cutting zone. The tissue response of particle  $i$  is parameterized by  $k_c^i$ : the closer the tissue particle to the needle tip, the stronger the tissue reaction. The total cutting force exerted by the needle tip depends on the sum of all the  $n$  particles reaction. Let note  $d_c^i$  the distance between a particle  $i$  inside the cutting zone and the needle tip. At each time step, the intensity  $C$  of the tissue reaction against cutting force is equal to:

$$C = \frac{\sum_{i=1}^n k_c^i d_c^{i-1}}{\sum_{i=1}^n d_c^{i-1}} \quad (5)$$

The direction of the cutting force is set to be parallel to the needle shaft.  $d_c^i = 0$  means that the tissue particle is at the same position as the needle particle: only this tissue particle  $i$  is used to compute the cutting force.

The cutting force intensity applied on each tissue particle  $i$  is then  $(k_c^i d_c^{i-1}) / (\sum_{j=1}^n d_c^{j-1})$ . The forces applied on the tissue particles are opposite to the force applied on the needle

node. During retraction of the needle, no more cutting forces are applied on the tissue.

### Friction force

The same principle is used for the friction force. As there is one friction zone per needle node, the tissue reaction to the friction depends locally on the tissue particles inside the friction zones. Let us consider one friction zone around one needle node. Let  $n$  be the number of particles in this friction zone,  $k_f^i$  be the friction force parameters of these  $n$  particles, and  $d_f^i$  the distance between particle  $i$  and the considered needle node. At each time step, the intensity  $F$  of the tissue reaction against friction force is equal to:

$$F = \frac{\sum_{i=1}^n k_f^i d_f^{i-1}}{\sum_{i=1}^n d_f^{i-1}} \quad (6)$$

Similarly, the friction force intensity applied on each tissue particle  $i$  is then  $(k_f^i d_f^{i-1}) / (\sum_{j=1}^n d_f^{j-1})$ . The direction of the friction force is parallel to the needle shaft.

Our approach to model static and kinetic friction force is based on the definition given by [BW98]. When the tangential velocity of a node along the needle shaft and the velocity of the needle are smaller than a given threshold, then static friction is applied: the tissue and the needle are moving together. When the tangential force required to move the tissue and the needle exceeds a slip force threshold, then tissue particles are free to slide along the needle shaft and only a friction force (along the needle axis) is applied on them.

**Virtual tissue particles** As there is not any remeshing in our model, tissue particles are not necessarily along the needle. Thus, a displacement constraint can not be directly applied on the tissue particles during the static friction (when tissue particles move at the same velocity than needle). The static friction in our model is achieved through *virtual tissue particles*. Each needle node carries a virtual tissue particle. At each iteration, the needle node position is considered as the undeformed position of the virtual particle. Thus the corresponding discrete deformation coordinates of this virtual particle are computed using the tissue particles belonging to the friction zone as neighbors. At the next iteration, the needle node and the tissue particles have moved: the shape memory attractor of the virtual tissue particle is computed again using the discrete deformation coordinates previously defined. A *virtual elastic force* is defined between the virtual tissue particle and its attractor.

If the intensity of this force is under the friction force threshold, the needle node is in a static friction state. The friction force and the elastic force are applied on the needle node. The opposite of the virtual elastic force is redistributed to the tissue particles as described in the paragraph 3.2.

**Puncture force** The puncture force is often described as an additional force to the cutting force that allows the needle tip to puncture the membrane of a soft organ. To define this soft

tissue property, the cutting force parameter is increased for the soft tissue external particles. The puncture force is thus defined for all possible location of the needle insertion.

### 4.2.2. Algorithm

The following algorithm details the computation steps of the new position for one needle.

---

**Algorithm 2:** Algorithm of one iteration for needle insertion modeling

---

```

foreach node of the needle do
  computeTissueForces();
  /* Punction, cutting and friction forces */
  computeVirtualElasticForce();
  if ( ||virtualElasticForce|| < ||frictionForce|| ) then
    /* Stick state */;
    redistributeTissueForces();
    redistributeVirtualElasticForce();
  else
    /* Slide state */;
    redistributeTissueForces();
  end
end
sumForces();
computeNeedleMovement();
adjustIntensityNeedleVelocity();

```

---

## 5. Simulation of Prostate Interventions

### 5.1. Medical Context

In this section, preliminary results of simulations of medical procedures around the prostate are presented. The influences of two particular instruments are studied: needles and ultrasound probe. These two instruments are commonly used in biopsy and brachytherapy (Figures 1 and 2). The influence of surrounding organs is also tested. The main organs around the prostate are the bladder and the rectum. Separations and connections between these organs can be considered as fat tissue. For the following simulations, the geometry of the organs was built from anatomical drawings. A general view of the complete model is represented in Figure 9.

Bladder and rectum are surface components (no internal particles) while prostate and fat tissues are volumetric components. Organ volumes are constrained for the prostate and bladder, which are both considered incompressible during the simulations.

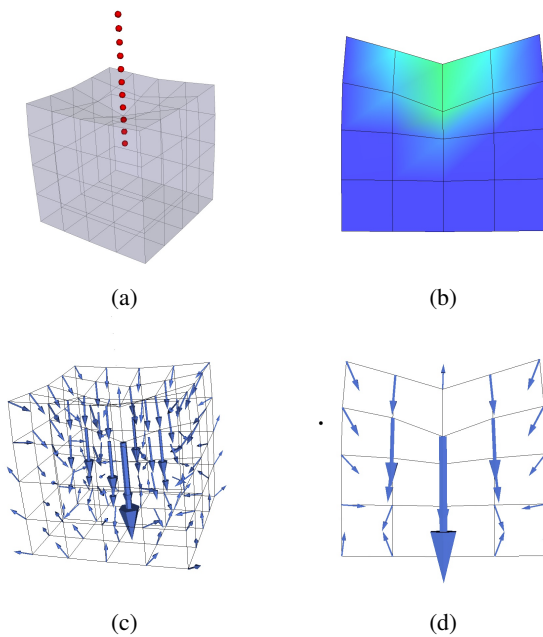


**Figure 8:** Simulation of the needle insertion in an elastic object: (a) Global view, (b) Displacements in the tissue (the green color corresponds to the highest displacements), (c) Forces applied on the tissue particles, (d) Details of the sum of forces applied on tissue particles in the middle slice of the cube.

## 5.2. Implementation details

The model is implemented in C++ using a Pentium M 2Ghz and compiling using gcc v4.1, without any particular effort to optimize code. Thanks to PML [CP04], geometry, organization, neighborhoods, physical properties and simulation loads are defined using a generic XML document.

Concerning time performances, for example for 125 particles (Figure 8), it takes a mean value of 9 ms for one iteration. For the complete model with 1300 particles (prostate, bladder and fat tissue), it takes 133 ms for one iteration.

## 5.3. Influence of Surrounding Organs

In this paragraph, the example of bladder filling influence is shown. The bladder, situated on top of the prostate, can induce some deformations and constrain prostate movements. The MRI images in Figure 10 show two different bladder fillings of the same subject before and after ingestion of one liter of water. The impact on the prostate deformation is clearly visible.

Different bladder volumes have been simulated and the deformations of the prostate observed. For example in Figure 11, the bladder volume is doubled. The figure shows the

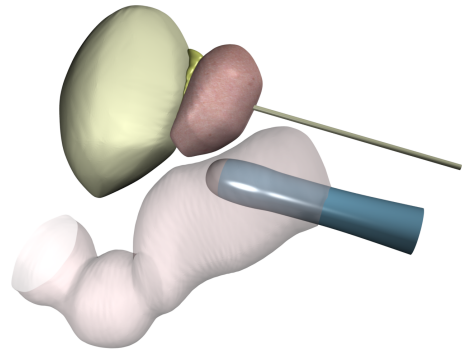


**Figure 9:** Complete anatomical model. Three organs are shown: prostate (red), bladder (yellow) and rectum (pink), and two surgical instruments (an ultrasound probe and a brachytherapy needle).

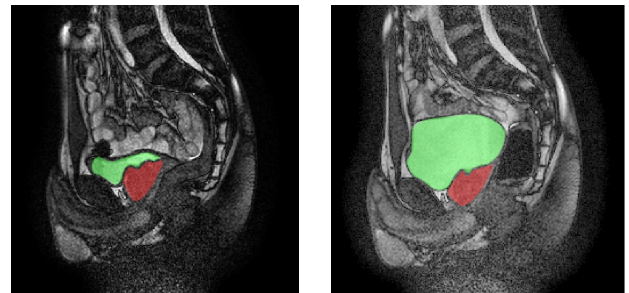


**Figure 10:** Different bladder fillings (green) and the influence on the prostate shape (red).

simulation results before and after the volume changes (other surrounding organs and boundary conditions are not represented in the figure). Prostate displacements observed during this bladder volume increase are presented in Figure 12. Displacements observed during an intervention are of the same order.

## 5.4. Influence of surgical Instruments

### 5.4.1. Ultrasound Probe

The influence of an endorectal ultrasound probe can also be simulated. The tissue displacements imposed by the surgeon through the probe in order to obtain the ultrasound images are translated as boundary conditions: displacements are imposed to the prostate particles directly in contact with the rectum particles in collision with the probe.

In the simulation, prostate deformations can be observed, especially during biopsy simulation where the probe is not parallel to the rectum wall. The probe simulations have also been combined with different bladder fillings. When the bladder volume is important, the prostate being more con-



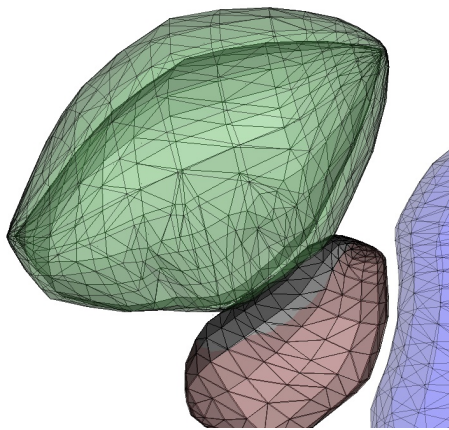


**Figure 11:** Different bladder volumes have been tested: the upper part of the prostate (red) is deformed when the bladder volume is nearly doubled.

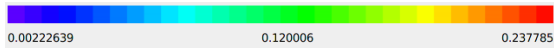
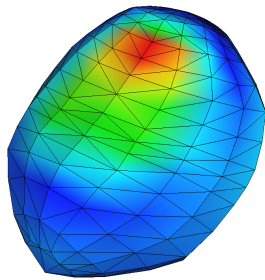


**Figure 12:** Prostate displacements during the bladder volume increase (the highest displacements are in red). Values are given in centimeters.

strained moves slightly while local deformations are higher. Other organ influences (like rectum filling) can also be tested with the model.

#### 5.4.2. Needles

The Figure 13 shows a real ultrasound image illustrating the influence of a needle on the prostate shape during a biopsy. For our simulations, a mean bladder volume is chosen and the ultrasound probe is simulated as a boundary condition. Simulations were made with two different orientations for the needles, mimicking two surgical procedures (biopsy and brachytherapy). The figures 14 and 15 show the simulations of needle insertions for both procedures.

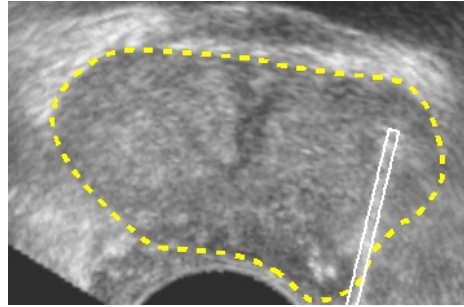


**Figure 13:** Influence of a needle on the prostate shape during a biopsy: the prostate boundaries are delimited in yellow while the needle is underlined with a blue color. The deformation occurs on the upper part of the prostate.

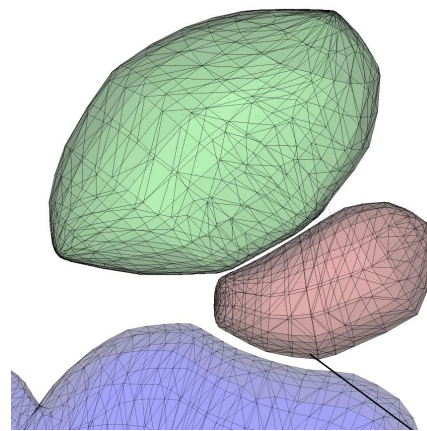


**Figure 14:** Insertion of a needle in a prostate through the rectum wall during a biopsy.

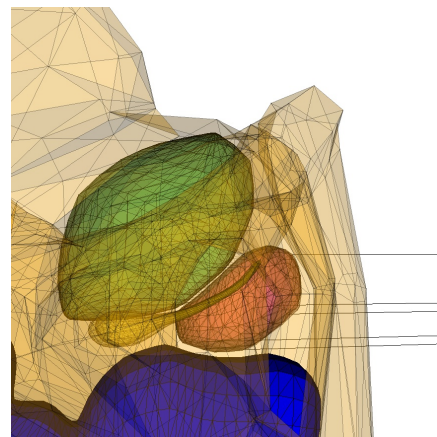


**Figure 15:** Insertion of several needles in a prostate during a brachytherapy. Bones are represented in a transparent color.

## 6. Conclusion and Future Work

In this paper, a discrete modeling method is proposed to simulate both internal interactions between different organs and external interactions between organs and surgical tools. The presented model exhibits realistic behaviors for the simulated organs and its discrete construction allows to easily combine different interactions together. It owns a specific formulation of elasticity whose performances were validated against other soft tissue modeling methods and real data. Thanks to the attractor principle, an algorithm based on a *virtual tissue particle* is able to simulate needle insertion. The modeling of flexible needles is currently tested and will enrich the simulator.

First results in the surgical simulation of prostate interventions are presented. Our framework can also be used for other medical simulations and different anatomical environments, especially ultrasound imaging guided biopsies. Our future work is to validate the simulator using phantoms and real data, aiming at building a simulator capable of valid and robust surgical planning.

## 7. Acknowledgment

The 3D geometry of the organs were built in collaboration with GRAVIR Laboratory (INRIA, Grenoble, France). The MRI images were obtained thanks to MRI unit of Pr. Lebas (Grenoble hospital).

## References

- [AGCO05] ALTEROVITZ R., GOLDBERG K., CHIRIKIJAN G., OKAMURA A.: Steering flexible needle under markov motion uncertainty. In *Proceedings of IEEE International Conference on Intelligent Robotic System* (2005), pp. 120–125. 110
- [AGO05] ALTEROVITZ R., GOLDBERG K., OKAMURA A.: Planning for steerable bevel-tip needle insertion through 2d soft tissue with obstacles. In *Proceedings of IEEE International Conference on Robotics and Automation (ICRA)* (2005), pp. 1652–1657. 114
- [APT\*03] ALTEROVITZ R., POULIOT J., TASCHEREAU R., HSU I., GOLDBERG K.: Needle insertion and radioactive seed implantation on human tissue: Simulation and sensitivity analysis. In *Proceedings of IEEE International Conference on Robotics and Automation (ICRA)* (2003), pp. 1793–1799. 110
- [BW98] BARAFF D., WITKIN A.: Large steps in cloth animation. In *Computer Graphics Proceedings, SIGGRAPH* (1998), pp. 43–54. 115
- [CP04] CHABANAS M., PROMAYON E.: Physical model language: Towards a unified representation for continuous and discrete models. In *Proceedings of International Symposium on Medical Simulation* (2004), pp. 256–266. 116
- [DS03] DIMAIO S., SALCUDEAN S.: Needle insertion modeling and simulation. *IEEE Transactions on Robotics and Automation* 19 (2003), 864–875. 114
- [DS05] DIMAIO S., SALCUDEAN S.: Interactive simulation of needle insertion models. *IEEE Transactions on Biomedical Engineering* 52 (2005), 1167–1179. 110
- [FHK06] FLOATER M., HORMANN K., KOS G.: A general construction of barycentric coordinates over convex polygons. *Advances in Computational Mathematics* 24 (2006), 311–331. 112
- [GS04] GLOZMAN D., SHOHAM M.: Flexible needle steering and optimal trajectory planning for percutaneous therapies. In *Proceedings of MICCAI* (2004), pp. 137–144. 110
- [GSD\*05] GOKSEL O., SALCUDEAN S., DIMAIO S., ROHLING R., MORRIS J.: 3d needle-tissue interaction simulation for prostate brachytherapy. In *Proceedings of MICCAI* (2005), pp. 827–834. 110, 114
- [ICCO04] III R. W., COWAN N., CHIRIKIJAN G., OKAMURA A.: Nonholonomic modeling of needle steering. In *Proceedings of International Symposium on Experimental Robotics* (2004), pp. 3337–3343. 110, 114
- [IKC\*06] III R. W., KIM J., COWAN N., CHIRIKIJAN G., OKAMURA A.: Nonholonomic modeling of needle steering. *The International Journal of Robotics Research* 25, 5-6 (2006), 509–525. 110
- [KCO\*03] KERDOK A., COTIN S., OTTENSMEYER M., GALEA A., HOWE R., DAWSON S.: Truthcube : Establishing physical standards for real time soft tissue simulation. *Medical Image Analysis* 7 (2003), 283–291. 113
- [MDT02] MOHAMED A., DAVATZIKOS C., TAYLOR R.: A combined statistical and biomechanical model for estimation of intra-operative prostate deformation. In *Proceedings of MICCAI* (2002), pp. 452–460. 110
- [MHTG05] MÜLLER M., HEIDELBERGER B., TESCHNER M., GROSS M.: Meshless deformations based on shape matching. In *Proceedings of SIGGRAPH* (2005), pp. 471–478. 112
- [MPT05] MARCHAL M., PROMAYON E., TROCCAZ J.: Simulating complex organ interactions: Validation of a soft tissue discrete model. In *Proceedings of International Symposium on Visual Computing* (2005), pp. 175–182. 113
- [PA04] PADILLA M., ARAMBULA F.: Three-dimensional deformable model of the prostate for turp surgery simulation. *Computers & Graphics* 28 (2004), 767–777. 110
- [SO02] SIMONE C., OKAMURA A.: Modeling of needle insertion forces for robot-assisted percutaneous therapy. In *Proceedings of IEEE International Conference on Robotics and Automation (ICRA)* (2002), pp. 2085–2091. 114